Electronic Supplementary Information

Photoswitching of the Second-order Nonlinearity of a Tetrahedral Octupolar Multi DTE-based Copper(I) Complex

Hiroyuki Nitadori, Lucie Ordronneau, Julien Boixel, Denis Jacquemin, Abdou Boucekkine, Anu Singh, Munetaka. Akita, Isabelle Ledoux, Véronique Guerchais and Hubert Le Bozec

General information. All manipulations were performed using Schlenk techniques under an Ar atmosphere. All solvents were dried and purified by standard procedures. Spectroscopic grade dichloromethane was used for all optical measurements. NMR spectra were recorded on Bruker DPX-200, AV 300 or AV 500 MHz spectrometers. ^{1}H and ^{13}C chemical shifts are given versus $SiMe_4$ and were determined by reference to residual ^{1}H and ^{13}C solvent signals. Attribution of carbon atoms was based on HMBC, HMQC and COSY experiments. High resolution mass spectra (HRMS) were performed on a MS/MS ZABSpec TOF at the CRMPO (Centre de Mesures Physiques de l'Ouest) in Rennes. Elemental analyses were performed at the CRMPO.

Synthesis

6,6'-dimethyl-4,4'-bis((trimethylsilyl)methyl)-2,2'-bipyridine : To a THF solution (40 mL) of diisopropylamine (1.5 mL, 10.6 mmol) at -78 °C was added ^{n}BuLi (1.6M in hexane, 6.4 mL, 10.2 mmol) *via* a syringe. The solution was then stirred for 40 min and a solution of 6,6',4,4'-tetramethyl-2,2'-bipyridine (0.80 g, 3.8 mmol) in THF (50 mL) was added dropwise at -78 °C. The red-brown mixture was stirred for 40 min at -78 °C , 45 min at -10 °C and then was cooled to -78 °C before addition of TMSCl (1 mL, 7.9 mmol). The reaction was quenched with EtOH (20 mL) 15 s after TMSCl addition. Saturated aqueous $NaHCO_3$ (40 mL) was added to the reaction mixture, which was then allowed to warm to room temperature. The product was extracted with ethyl acetate (120 mL), and then combined organic fractions were washed with water (3 x 50 mL) and dried over $MgSO_4$. After filtration and removal of the solvent under vacuum, the compound was obtained as a yellow powder (1.09 g, 81 %). RMN ^{1}H (200 MHz, $CDCl_3$) δ ppm : 7.76 (s, 2H, Py^3), 6.80 (s, 2H, Py^5), 2.58 (s, 6H, CH_3), 2.17 (s, 4H, CH_2), 0.05 (s, 18H, TMS).

4,4'-bis(chlorométhyl)-6,6'-diméthyl-2,2'-bipyridine 2 : To 6,6'-dimethyl-4,4'bis((trimethylsilyl)methyl) 2,2'-bipyridine (1.1 g, 3 mmol) and hexachloroethane (2.9 g, 12.1 mmol) in CH_3CN (20 mL) was added cesium fluoride (1.8 g, 12.1 mmol). The solution stirred at 60 °C for 16h. After addition of ethyl acetate (40 mL) and water (40 mL), the organic layer was washed with water (3 x 50 mL), dried over $MgSO_4$, filtered and concentrated under vacuum. The resulting solid was finally washed with pentane to afford compound **2** as a white powder (0.692 g, 82 %). ^{1}H NMR (200 MHz, $CDCl_3$) δ ppm : 8.24 (s, 2H, Py^3), 7.26 (s, 2H, Py^5), 4.62 (s, 4H, CH_2), 2.67 (s, 6H, CH_3). ^{13}C [^{1}H] NMR (100 MHz, $CDCl_3$) δ ppm : 158.86, 156.13, 147.10, 122.71, 117.84, 44.59, 24.73. Anal. Calcd. for $C_{14}H_{14}N_2Cl_2$. $0.5H_2O$: C, 57.95; H, 5.21; N, 9.65. Found: C, 58.59; H, 4.96; N, 9.52.

6,6'-dimethyl-4,4'-bis(diethylphosphonomethyl)-2,2'-bipyridine 3. Freshly distilled diethylphosphite (2.0 mL, 15.5 mmol) was added dropwise to a solution of NaH (0.368 g, 15.3 mmol) in toluene (20 mL) at 0° C. The reaction mixture was heated for 1h at 80 °C. Then, a solution of 4,4'-bis(chloromethyl)-6,6'-dimethyl-2,2'-bipyridine **2** (0.540 g, 1.9 mmol) in toluene (10 mL) was added, and the reaction mixture was heated at 80 °C for 22h. The solution was then allowed to cool down to room temperature. After addition of brine (40 mL) and ethyl acetate (40 mL), the organic layer was washed with water (3 x 20 mL), dried over $MgSO_4$, filtered and concentrated. Compound **3** was obtained as a bright yellow powder (0.621 g, 69 %). ^{1}H NMR (200 MHz, $CDCl_3$) δ ppm : 8.15 (s, 2H, Py^3), 7.14 (s, 2H, Py^5), 4.09 (q, ^{3}J = 8.0 Hz, 8H, OCH_2), 3.22 (d, $^{3}J_{H\text{-}P}$ = 22.0 Hz, 4H, CH_2), 2.62 (s, 6H, CH_3), 1.31 (t, ^{3}J = 6.0 Hz, 12 H, CH_3). ^{13}C [^{1}H] NMR (100 MHz, $CDCl_3$) δ ppm : 158.17, 158.15, 142.01, 141.92, 124.45, 124.39, 62.53, 62.46, 34.22, 32.86, 31.00, 24.60, 16.47, 16.41. Anal. Calcd. for $C_{22}H_{34}N_2O_6P_2$. H_2O: C, 52.59; H, 7.02; N, 5.58. Found: C, 52.43; H, 6.52; N, 6.03.

6,6'-dimethyl-4,4'-bis((E)-2-(4-(3,3,4,4,5,5-hexafluoro-2-(2-methyl-5-*p*-N,N-dimethylaminophenyl-thiophen-3-yl)cyclopent-1-nyl)-5-methylthiophen-2-yl)vinyl)-2,2'-bipyridine, L_{oo}. A THF solution (25 mL) of 4-(3,3,4,4,5,5-hexafluoro-2-(2-methyl-5-N,N-dimethylaminophenylthiophenyl-3)cyclopent-1-enyl)-5 methylthiophene -2-carbaldehyde (0.237 g, 0.50 mmol) was added to **3** (0.119 g, 0.20 mmol) and ^{t}BuOK (0.107

g, 0.90 mmol) at 0°C. The reaction mixture was stirred overnight at room temperature. After addition of water, the organic layer was washed with brine and water, dried over $MgSO_4$, filtered and concentrated. Crystallization in a CH_2Cl_2-pentane mixture afforded **L** as a brown powder (0.189 g, 68 %). ^{1}H NMR (400 MHz, $CDCl_3$) δ ppm : 8.35 (s, 2H, Py^3), 7.52 (d, ^{3}J = 16.1 Hz, 2H, =CH), 7.46 (d, ^{3}J = 8.9 Hz, 4H, C_6H_4-), 7.26 (s, 2H, Py^5), 7.22 (s, 2H, thio), 7.15 (s, 2H, thio), 6.90 (d, ^{3}J = 16.1 Hz, 2H, =CH), 6.76 (d, ^{3}J = 8.9 Hz, 4H, C_6H_4-), 3.01 (s, 12H, N*Me*$_2$), 2.67 (s, 6H, CH_3^{bipy}), 2.04 (s, 6H, CH_3), 2.00 (s, 6H, CH_3). ^{13}C [^{1}H] NMR (100 MHz, CD_2Cl_2) δ (ppm) : 158.38, 155.91, 150.38, 145.10, 143.37, 142.74, 139.97, 139.35, 127.37, 126.53, 126.41, 125.70, 125.35, 124.95, 121.34, 120.01, 119.65, 115.17, 112.31, 40.11, 24.23, 14.60, 14.22. HRMS: m/z 1207.2810 $[M+H]^+$, calcd for $C_{62}H_{51}N_4F_{12}S_4$ 1207.2805. Anal. Calcd. for $C_{62}H_{50}F_{12}N_4S_4.3CH_2Cl_2$: C, 53.39; H, 3.86; N, 3.83. Found: C, 53.08; H, 4.07; N, 3.66.

Spectroscopic data of the photocyclized $\mathbf{L_{c,c}}$**.** ^{1}H NMR (300 MHz, CD_2Cl_2) δ (ppm) : 8.40 (s, 2H, Py^3), 7.52 (d, ^3J = 8.88 Hz, 4H, Ph), 7.50 (d, ^3J = 16.08 Hz, 2H, $=CH^8$), 7.27 (s, 2H, Py^5), 6.78 (d, ^3J=16.08 Hz, 2H, $=CH^7$), 6.72 (d, ^3J=8.88 Hz, 4H, Ph), 6.63 (s, 2H, Thio), 6.54 (s, 2H, Thio), 3.11 (s, 12H, NMe_2), 2.69 (s, 6H, CH_3^{bpy}), 2.18 (s, 6H, CH_3), 2.16 (s, 6H, CH_3).

$[Cu(L_{o,o})_2]PF_6$. To a CH_3CN/CH_2Cl_2 solution (5/10 mL) of $\mathbf{L_{o,o}}$ (0.162 g, 0.134 mmol) was added $[Cu(CH_3CN)_4]PF_6$ ((0.025 g, 0.067 mmol). The reaction mixture was stirred for 3 days at room temperature. The solvent was then evaporated and crystallization of the residue in a CH_2Cl_2/pentane mixture afforded a brown powder (0.172 g, 97 %). ^{1}H NMR (400 MHz, CD_2Cl_2) δ ppm : 8.19 (s, 4H, Py^3), 7.61 (d, ^3J = 16.0 Hz, 4H, $=CH^8$), 7.47 (s, 4H, Py^5), 7.45 (d, ^3J = 8.0 Hz, 8H, Ph), 7.29 (s, 4H, Thio), 7.12 (s, 4H, Thio), 6.92 (d, ^3J = 16.0 Hz, 4H, $=CH^7$), 6.71 (d, ^3J = 8.0 Hz, 8H, Ph), 2.97 (s, 24H, NMe_2), 2.25 (s, 12H, CH_3^{bpy}), 2.03 (s, 12H, CH_3), 1.96 (s, 12H, CH_3). ^{13}C [^{1}H] NMR (100 MHz, $CDCl_3$) δ ppm : 157.00, 152.32, 150.41, 143.74, 143.44, 139.44, 128.89, 127.61, 126.71, 126.24, 125.51, 124.79, 121.72, 119.82, 112.62, 40.55, 29.84, 25.22, 15.02, 14.61, Anal. Calcd. for $C_{124}H_{100}F_{30}N_8P_1S_8Cu.2CH_2Cl_2$: C, 54.18; H, 3.75; N, 4.01. Found: C, 54.02; H, 3.93; N, 4.18.

Spectroscopic data of the photocyclized **$[Cu(L_{c,c})_2]PF_6$**. ^{1}H NMR (500 MHz, CD_2Cl_2) δ ppm : 8.21 (s, 4H, Py^3), 7.54 (d, ^3J = 16.0 Hz, 4H, $=CH^8$), 7.51 (s, 4H, Py^5), 7.46 (d, ^3J = 8.0 Hz, 8H, Ph), 6.76 (d, ^3J = 16.0 Hz, 4H, $=CH^7$), 6.75 (d, ^3J = 8.0 Hz, 8H, Ph), 6.65 (s, 4H, Thio), 6.65 (s, 4H, Thio), 3.12 (s, 24H, NMe_2), 2.28 (s, 12H, CH_3^{bpy}), 2.21 (s, 12H, CH_3), 2.20 (s, 12H, CH_3).

Optical spectroscopy.

UV-vis irradiations were performed either with a Rayonet photochemical reactor RPR 100 equipped with 16 RPR 3500 Å lamps, or with a LS series Light Source of ABET technologies, Inc (150 W xenon lamp), with single wavelength light filters of “350FS 10-25”, “450FS 20-25” and “650FS 10-25”. UV/vis absorption spectra were recorded using a UVIKON 9413 or Biotek Instruments XS spectrophotometer using quartz cuvettes of 1 cm pathlength (Spectroscopic grade dichloromethane was used for all optical measurements).

Theoretical Calculations

A. Methodology

To perform our simulations, we have selected the latest version of the Gaussian program.[1] The *ab initio* simulations consisted in geometry optimization and subsequent TD-DFT calculations of the different isomers using all possible closed/open combinations for the four photochromes. We have considered only the anti-parallel conformers here, as the parallel DTE structures are known to be non-photochromic. We have applied default procedures, integration grids, algorithms and parameters, except for tighten energy (10^{-9} a.u.) and internal forces (10^{-5} a.u.) convergence thresholds. The ground-state geometrical parameters have been determined at the PBE0/6-31G(d) level,[2] via a force-minimization process. For the two fully symmetric structures $[Cu(\mathbf{L_{o,o}})_2]^+$ and $[Cu(\mathbf{L_{c,c}})_2]^+$, the vibrational spectrum has been determined analytically at the same level of theory and it has been checked that all structures correspond to true minima of the potential energy surface. At least, the first eighteen low-lying excited-states have been determined within the vertical TD-DFT approximation using the CAM-B3LYP/6-31+G(d) level of approximation,[3] as this range-separated hybrid has been shown adequate for investigating multi-DA architectures.[4] In this latter step, a modeling of bulk solvent effects (here CH_2Cl_2) through the Polarizable Continuum Model (PCM).[5] Note that only PCM-CAM-B3LYP/6-31+G(d) orbitals are shown here. The simulated UV/Vis spectra use a broadening Gaussian of 0.35 eV of FWHM whereas the contour threshold for the orbitals was set to 0.02 a.u. The first hyperpolarizability (β) tensor was computed analytically using a CP-KS procedure and a PCM-ωB97X/6-31+G(d) approach.[6] An ultrafine DFT integration grid was applied to allow proper convergence. The selection of a range-separated hybrid with correct asymptotic behavior was motivated by previous works demonstrating the importance of long-range effects for calculation of β.[7,8]

B. Basis set benchmark

For the records, we have recomputed the geometric and spectral data using larger basis sets for $[Cu(\mathbf{L}_{o,o})_2]^+$ and $[Cu(\mathbf{L}_{c,c})_2]^+$ and it provided completely similar results. Indeed, these two molecules belong to the D_2 point group and extra calculations could be performed, using the 6-311G(d,p) and 6-311+G(2d,p) basis sets, for the ground-state and excited-state properties, respectively, as well as applying the LanL08 pseudopotential and basis set for the central copper atom. This combination is known to provide fully converged properties optical for DTE.[9] With these extended choice, the first band of $[Cu(\mathbf{L}_{o,o})_2]^+$ presenting with an oscillator strength larger than 0.5 is centered at 420 nm, whereas the estimate with the "standard" basis set is 438 nm. The discrepancy is even smaller for the λ_{max} of $[Cu(\mathbf{L}_{c,c})_2]^+$, located at 685 nm with 6-311+G(2d,p), a value completely alike its 6-31+G(d) counterpart (692 nm).

C. Extra analysis

$[Cu(\mathbf{L}_{o,o})_2]^+$ and $[Cu(\mathbf{L}_{c,c})_2]^+$ belong to the D_{2d} and the angle between the two ligands are close to 90°. The relevant results required to analyze the optical spectra and DTE features are collated in Table S1. For the doubly-open doubly-closed case, we have investigated both the structure presenting the closed DTE on the same ligand, $[Cu(\mathbf{L}_{o,o})(\mathbf{L}_{c,c})]^+$ and the isomer with closed DTE on two different ligands, $[Cu(\mathbf{L}_{o,c})_2]^+$. As expected for DTE, the successive photo-cyclizations, that yield to the closed isomers, imply an energetic cost. We estimate this penalty to be ca. 6 kcal.mol^{-1} per switched photochromic unit and to be linearly dependent of the number of closed DTE. This latter point is well-illustrated by the relative total ground-state energy of $[Cu(\mathbf{L}_{c,c})_2]^+$ (24.6 kcal.mol^{-1}) that is nearly exact four times its $[Cu(\mathbf{L}_{o,o})(\mathbf{L}_{o,c})]^+$ counterpart (6.3 kcal.mol^{-1}). This 6.3 kcal.mol^{-1} value is similar to the one found in other architectures containing one or more DTE,[4,10,11] and remains relatively small compared to significantly constrained multi-color structures.[12] Therefore, there is no indication of a strong dependency between the DTE units on the ground-state energetic basis, nor hints of a specifically unstable product. The same conclusion holds for the geometric parameters with distances between the two reactive carbons atoms that are standard for both open (3.5–3.6 Å) and closed (1.55 Å) DTE. It is worth to notice, that the CC distances of the open DTE remain well below the 4.2 Å threshold that is known to be problematic for photochromism, at least in the solid-state.[13]

Previous theoretical analysis of the photochemistry of isolated diarylethene models have demonstrated the importance of conical intersections,[14,15] and therefore the impact of several electronic excited-states potential energy surfaces,[14–18] in the various photochromic processes involved in such switches. Unfortunately, such involved investigations are not computationally tractable for the present case (> 250 atoms, > 3000 basis functions), and we have to go for a more quali- tative model. In previous investigations on photochromic dimers and trimers, it has been shown that an analysis of the topology of the virtual molecular orbitals (MO) of the different isomers may give insights into the photo-reactivity, though such analysis remains crude and also has it flaws.[19-21] In Figure S1, we present the evolution with successive electro-cyclization of the MO energies. The "*photochromic orbitals*", that is the virtual MOs centered on the open DTE and characterized by both a bonding nature for the to-be-formed carbon-carbon bond and a significant density on (at least one of) the two reactive carbon atoms (see Figure S4), have been identified. These virtual orbitals have a topology similar to the highest occupied orbitals of the closed DTE, and are important for the electro-cyclization of the systems in the MO picture. It is clear from Figure S2 that the energy of these photochromic orbitals are almost unaffected by the successive DTE ring-closure, i.e. they present the same energy for each open DTE irrespective of the status of other DTE.

D. NLO calculation results

Using the above-described procedure, we calculate static electronic β_{xyz} values of 77 x 120^{-30} esu and 564 x 10^{-30} esu for $[Cu(\mathbf{L}_{o,o})_2]^+$ and $[Cu(\mathbf{L}_{c,c})_2]^+$, respectively. The enhancement factor is therefore very consistent with experimental measurements, further supporting a full cyclizations of all DTE. Of course, the absolute values do not exactly match the experimental reference, an expected fact for this kind of molecules, that can be partially explainable by the selected functionals (that is qualitatively but not necessarily quantitatively optimal), relatively compact basis set and solvent models.

HLS measurements.

The Harmonic Light Scattering (HLS) technique[22,23] involves the detection of the incoherently scattered second harmonic light generated by a solution of the molecule under irradiation with a laser of wavelength λ, leading to the measurement of the mean value of the β x β tensor product, $<\beta^2_{HLS}>$. All HLS measurements were carried out in CH_2Cl_2 solution at a concentration of 1×10^{-3} M, working with a low-energy, non-resonant incident radiation of 1.91 μm. The 1.91 μm fundamental beam was emitted by a high-pressure (30 bar), 50 cm long hydrogen-filled Raman cell pumped by a Nd^{3+}:YAG laser operating at 1.06 μm and providing a 10 Hz repetition rate, and pulses of 15 ns duration. Only the back-scattered 1.91 μm stimulated Raman emission was collected by use of a dichroic mirror, in order to eliminate most of the residual 1.06 μm pump photons. Our reference sample was a concentrated (10^{-3} M) solution of ethyl violet, its β value being 170 x 10^{-30} esu at 1.91 μm. The HLS photons at

955 nm were focused onto the photomultiplier tube using two collecting lenses (we used a Hamamatsu R632-01 photomultiplier tube). The signal detected was then sampled and averaged using a boxcar, and processed by a computer. The reference beam was collected at a 45° incidence angle by a glass plate, and focused onto a highly nonlinear NPP powder, which was used as the frequency doubler. The variation of the scattered second harmonic intensity from the solution was recorded on the computer as a function of the reference second harmonic signal provided by the NPP powder, which scales as the square of the incoming fundamental intensity. Values for β were then inferred from the slopes of the resulting lines. The microscopic β^2_{xyz} coefficient can be inferred from the statistical averaging relation $\langle\beta^2_{HLS}\rangle = 4/7\ \beta^2_{xyz}$.[24]

References

(1) Frisch, M. J. et al. Gaussian 09 Revision A.02, 2009, Gaussian Inc. Wallingford CT.
(2) Adamo, C.; Barone, V. *J. Chem. Phys.* 1999, **110**, 6158–6170.
(3) Yanai, T.; Tew, D. P.; Handy, N. C. *Chem. Phys. Lett.* 2004, **393**, 51–56.
(4) Jacquemin, D.; Perpète, E. A.; Maurel, F.; Perrier, A. *J. Phys. Chem. C* 2010, **114**, 9489– 9497.
(5) Tomasi, J.; Mennucci, B.; Cammi, R. *Chem. Rev.* 2005, **105**, 2999–3094.
(6) Chai, J. D.; Head-Gordon, M. *J. Chem. Phys.* 2008, **128**, 084106.
(7) Kamiya, M.; Sekino, H.; Tsuneda, T.; Hirao, K. *J. Chem. Phys.* 2005, **122**, 234111.
(8) Jacquemin, D.; Perpète, E. A.; Medved, M.; Scalmani, G.; Frisch, M. J.; Kobayashi, R.; Adamo, C. *J. Chem. Phys.* 2007, **126**, 191108.
(9) Jacquemin, D.; Perpète, E. A. *Chem. Phys. Lett.* 2006, **429**, 147–152.
(10) Patel, P. D.; Masunov, A. E. *J. Phys. Chem. C* 2011, **115**, 10292–10297.
(11) Perrier, A.; Maurel, F.; Aubard, J. J. *Photochem. Photobiol. A: Chem*. 2007, **189**, 167–176.
(12) Perrier, A.; Maurel, F.; Jacquemin, D. *J. Phys. Chem. C* 2011, **115**, 9193–9203.
(13) Kobatake, S.; Uchia, K.; Tsuchida, E.; Irie, M. *Chem. Commun*. 2002, 2804–2805.
(14) Boggio-Pasqua, M.; Ravaglia, M.; Bearpark, M. J.; Garavelli, M.; Robb, M. A. *J. Phys. Chem. A*. 2003, **107**, 11139–11152.
(15) Asano, Y.; Murakami, A.; Kobayashi, T.; Goldberg, A.; Guillaumont, D.; Yabushita, S.; Irie, M.; Nakamura, S. *J. Am. Chem. Soc*. 2004, **126**, 12112–12120.
(16) Mikhailov, I. A.; Belfield, K. D.; Masunov, A. E. *J. Phys. Chem. A* 2009, **113**, 7080–7089.
(17) Patel, P. D.; Mikhailov, I. A.; Belfield, K. D.; Masunov, A. E. *Int. J. Quantum Chem.* 2009, **109**, 3711–3722.
(18) Patel, P. D.; Masunov, A. E. *J. Phys. Chem. C* 2011, **115**, 10292–10297.
(19) Jacquemin, D.; Perpète, E. A.; Maurel, F.; Perrier, A. *J. Phys. Chem. C* 2010, **114**, 9489– 9497.
(20) Perrier, A.; Maurel, F.; Jacquemin, D. *J. Phys. Chem. C* 2011, **115**, 9193–9203.
(21) Jacquemin, D.; Perpète, E. A.; Maurel, F.; Perrier, A. *J. Phys. Chem. Lett.* 2010, **1**, 2104– 2108.
(22) Ledoux, I.; Zyss, J. *Chem. Phys.* 1982, **73**, 203-213.
(23) (a) Maker, P.D. *Phys. Rev. A.* 1970, **1**, 923-951. (b) Clays, K.; Persoons, A. *Phys Rev Lett.* 1991, **66**, 2980-2983. (c) Zyss, J.; Ledoux, I. *Chem. Rev.* 1994, **94**, 77-105.
(24) (a) Cyvin, S.G., Rauch, J.E., Decius, J.C. *J. Chem. Phys.* 1965, **43**, 4083; (b) Bersohn, R., Pao, Y.H., Frisch, H.L. *J. Chem. Phys*. 1966, **45**, 3184.

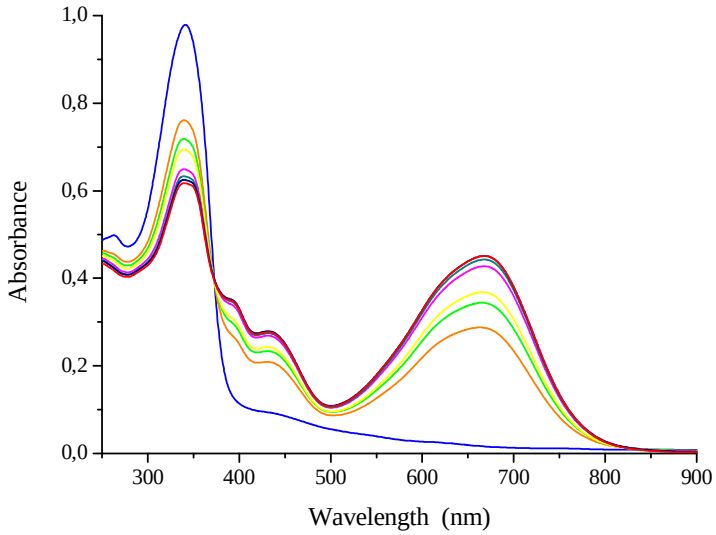

Figure S1. Experimental UV-vis absorption spectra change of $\mathbf{L}_{o,o}$ in dichloromethane upon excitation at 350 nm.

Table S1: Relative total energies (E in kcal.mol^{-1}), distances separating the reactive carbon atoms (d_i in Å) and relevant vertical transition wavelengths (λ in nm and the corresponding oscillator strengths, *f*). The two former are obtained at the PBE0/6-31G(d) level whereas the latter are computed with the PCM-TD-CAM-B3LYP/6-31+G(d) approach.

Isomer	***E***	d_1	d_2	d_3	d_4	λ	*f*
$[Cu(\mathbf{L}_{c,c})_2]^+$	24.60	1.54	1.54	1.54	1.54	692	1.53
						692	1.51
						690	1.66
						449	0.61
						389	0.39
						389	0.27
						380	0.41
						380	0.48
$[Cu(\mathbf{L}_{c,c})(\mathbf{L}_{o,c})]^+$	18.51	1.54	1.54	1.54	3.58	692	1.57
						689	1.48
						665	0.49
						447	0.78
						388	0.37
						379	0.40
$[Cu(\mathbf{L}_{o,o})(\mathbf{L}_{c,c})]^+$	12.17	1.54	1.54	3.58	3.58	695	1.54
						676	0.84
						454	0.33
						444	0.59
						390	0.31
						380	0.44
						373	1.56
						354	0.64
						346	0.35
$[Cu(\mathbf{L}_{o,c})_2]^+$	12.36	1.54	1.54	3.58	3.59	691	1.61
						675	0.77
						446	1.05
						384	0.33
						364	1.66
						363	1.22
						346	0.60
$[Cu(\mathbf{L}_{o,o})(\mathbf{L}_{o,c})]^+$	6.28	1.54	3.58	3.58	3.58	687	1.21
						437	0.98
						384	0.31
						373	1.63
						365	1.40
						346	0.32
						339	0.58
						338	0.37
$[Cu(\mathbf{L}_{o,o})_2]^+$	0.00	3.59	3.59	3.59	3.59	470	0.17
						438	1.37
						374	1.61
						373	1.53
						341	2.12

Figure S2: Representation of the orbital energies for the four highest occupied and ten lowest unoccupied orbitals. The photochromic orbitals are indicated by the red square (see text for more details).

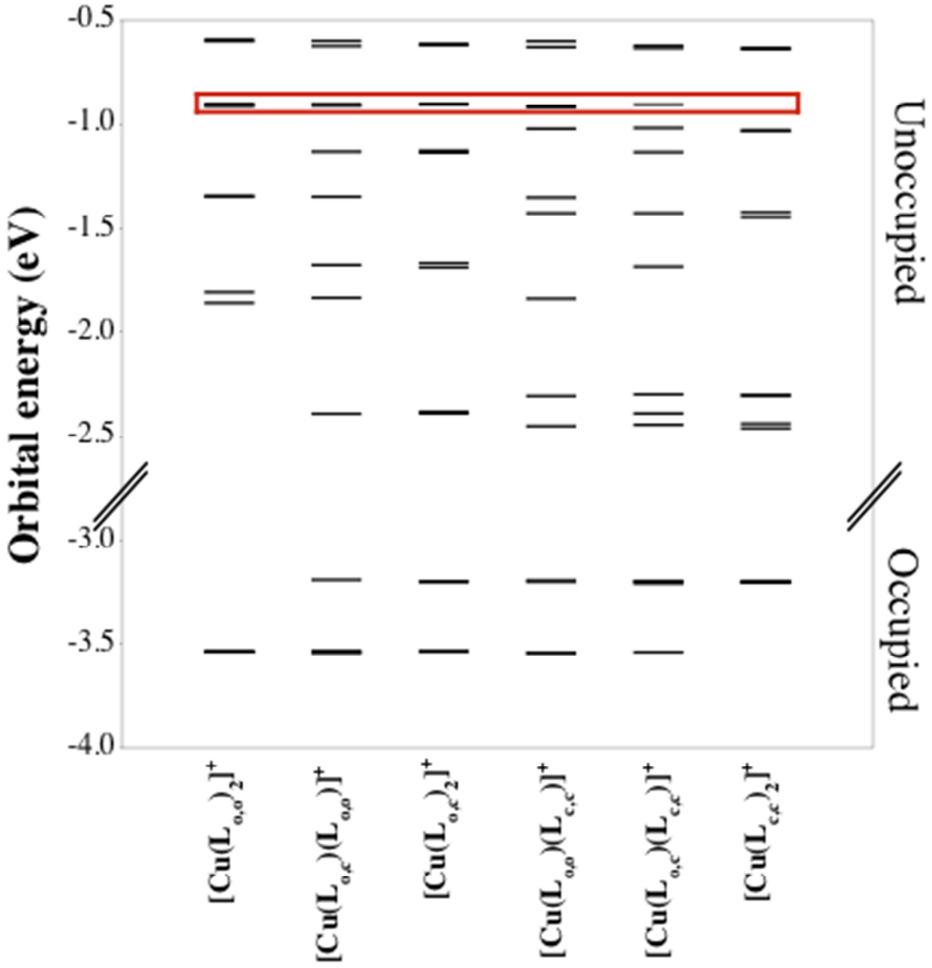

Figure S3: HOMO (left) and LUMO (right) of $[Cu(\mathbf{L}_{o,o})_2]^+$, $[Cu(\mathbf{L}_{o,o})(\mathbf{L}_{c,c})]^+$, $[Cu(\mathbf{L}_{c,c})_2]^+$ (from bottom to top).

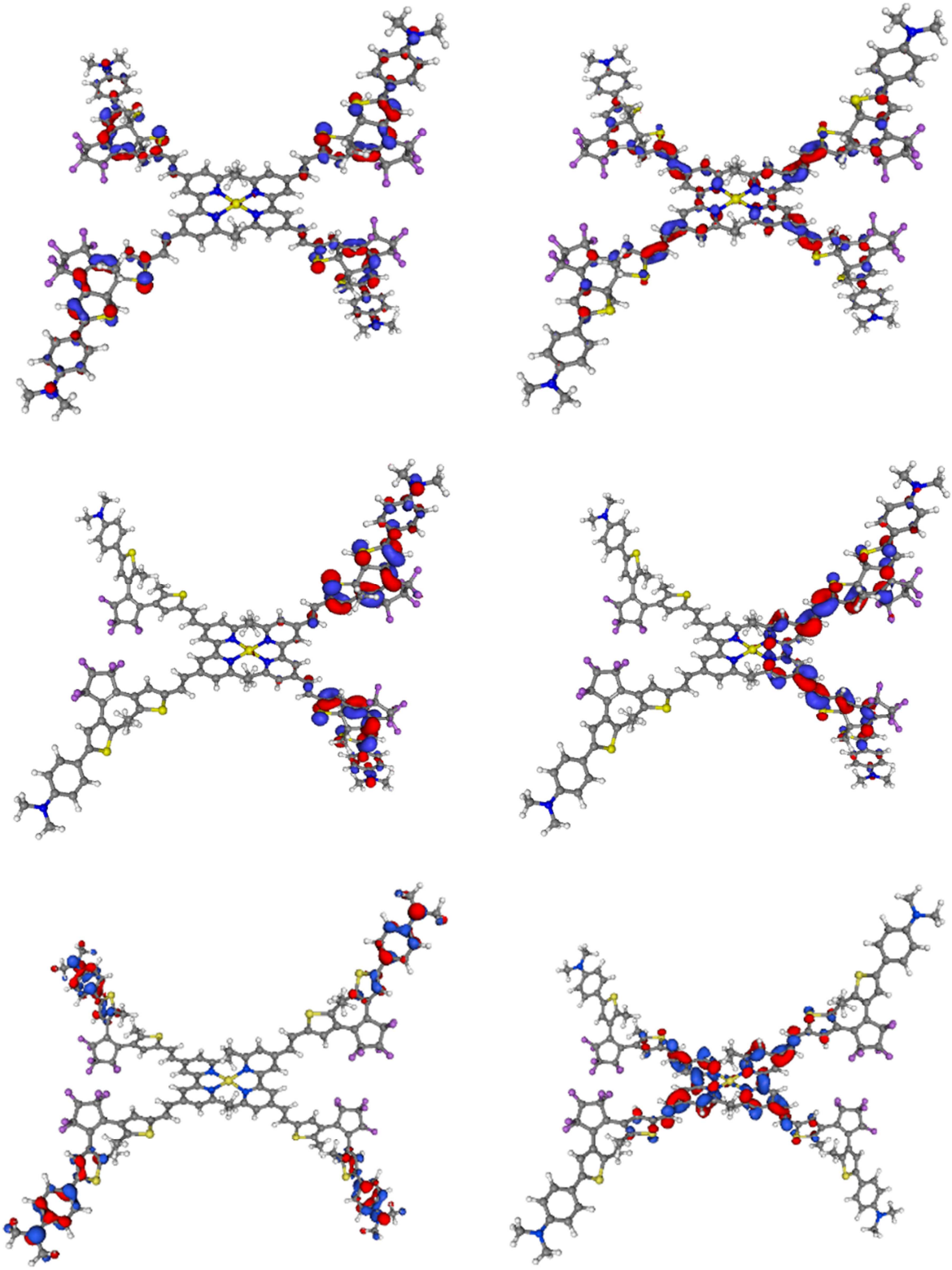

Figure S4: LUMO+4 of $[Cu(\mathbf{L}_{o,o})_2]^+$ as an illustration of a "photochromic orbital".